Crystallographic and hyperfine parameters of $PrTi(Fe,Co)_{11}$ and their carbides

L. Bessais, S. Sab, and C. Djéga-Mariadassou
LCMTR, UPR209, CNRS, 2/8 rue Henri Dunant, BP 28, F-94320 Thiais, France

J. M. Grenèche
Laboratoire de Physique de l'État Condensé, UMR CNRS 6087, Université du Maine, F-72085 Le Mans, France

(Received 17 January 2002; published 20 August 2002)

$PrTiFe_{11-x}Co_x$ alloys ($x \leqslant 3$) prepared by melting and subsequent annealing have been investigated with their carbides $PrTiFe_{11-x}Co_xC_y$ ($y=1$) synthesized by means of reaction with solid hydrocarbon at 750 K. X-ray diffraction analysis by Rietveld method has shown that both series crystallize in the tetragonal $ThMn_{12}$-type structure. From x-ray studies of magnetic aligned samples, the magnetic anisotropy of the carbided alloys is found to turn uniaxial. Their Curie temperature enhancement is linearly correlated to the volume expansion of the host lattice upon carbonation. The Mössbauer spectra recorded from 77 to 293 K, have been analyzed on the basis of the binomial law, related to the different Fe nearest neighbor in the assumption of Ti atoms distributed in $8i$ sites. The hyperfine parameter sets were assigned according to the relationship between the Wigner Seitz cell volume of each iron site and their isomer shift δ so that $\delta\{8i\} > \delta\{8j\} > \delta\{8f\}$. It results that Co preferentially occupies the $8f$ site with the recurrent sequence $H_{HF}\{8i\} > H_{HF}\{8f\} > H_{HF}\{8j\}$. The increase with Co content of hyperfine field, is correlated to the increase of the core electron polarization field ruled by the asymmetrical filling of the $3d$ band by the additional $3d$ Co electron. Upon carbonation, both the hyperfine fields and the isomer shifts increase in agreement with the unit cell expansion and the increased Curie temperature of $PrTiFe_{11-x}Co_xC$ as compared to $PrTiFe_{11-x}Co_x$.

DOI: 10.1103/PhysRevB.66.054430 PACS number(s): 75.50.Bb, 75.50.Tt, 76.80.+y

I. INTRODUCTION

Rare-earth transition metal intermetallics $R-M$ are attractive compounds for their technological magnetic application. Most particularly, the RFe_{12} family has focused much attention due to the low ratio of rare-earth and high content of low cost iron. However, the tetragonal $ThMn_{12}$ structure, with space group $I4/mmm$, is not formed for any binary rare-earth iron intermetallic, but it must be stabilized by substitution of a small amount of Al or a transition metal such as Ti, V, Cr, Mo, W, etc. Consequently, there exists a great variety of magnetic properties according to the M solubility range and to the sign of the second-order Stevens coefficient α_J of the rare earth.[1]

$ThMn_{12}$ intermetallic structure possesses R_2Fe_4 octahedron units, which can be filled with nitrogen or carbon by solid-state diffusion in a low temperature gas-solid or solid-solid reaction. The anisotropy of rare-earth iron compounds is determined from the sum of the Fe sublattice anisotropy and the rare-earth sublattice anisotropy. The contribution of rare-earth sublattice to magnetocrystalline anisotropy arises from the coupling between rare-earth ion orbit magnetic moment and the crystal electric field. If the second-order field term is predominant, the anisotropy of rare-earth sublattice can be described by the product of the second-order crystal parameter A_{20} and the second-order Stevens coefficient α_J on the basis of single ion model.[2] A negative $\alpha_J A_{20}$ exhibits a uniaxial anisotropy. Extensive works have shown that the magnetocrystalline anisotropy was significantly modified by insertion of a small $2p$ element such as carbon or nitrogen, which expands the lattice.[3–11] This expansion modifies the A_{20} which becomes positive so that, for rare earth with negative α_J such as Nd or Pr, the c axis becomes easy. Especially, due to their relative high Curie temperature and favorable magnetization, these alloys may develop permanent magnet characteristics. However, the studies have been mainly performed up to now with $R=$Nd and $M=$Ti or Mo as the stabilizing metals.[6,11] When R is Pr, Mo was taken generally as the stabilizing element,[10,11] except in the work from Akayama *et al.*,[12] which reports structural and magnetic properties of induction melted $PrTiFe_{11}$ and its nitrides. The anisotropy field of $PrTiFe_{11}N_{1.5}$ was estimated to be higher than 7 T at room temperature but owing to the difficulties to get single phase $PrTiFe_{11}$, Tang *et al.* preferred recently to prepare the pseudoternary compound $PrFe_{11.5-x}V_xTi_{0.5}$ (Ref. 13). Interstitial carbon is expected to induce the same magnetic behavior as nitrogen. However, until now, few data about carbides are available for light rare-earth with negative α_J and concern $Nd(Fe,Mo)_{12}C_x$ (Ref. 3) or $Nd(Fe,Ti)_{12}C_x$ (Ref. 14). Nevertheless, the possibility of producing interesting hard permanent magnets is worth pursuing. Consequently, in this context, we have carried out the study of the $PrTiFe_{11-x}Co_x$ alloys ($x \leqslant 3$) with their recurrent carbides $PrTiFe_{11-x}Co_xC_y$ ($y=1$). The aim of the partial substitution of Fe for Co is mainly to increase their Curie temperature.[15]

Moreover, as the carbides do not exist at temperature up to 1373 K which is the annealing temperature required for the $PrTiFe_{11-x}Co_x$ alloy formation, it is necessary to prepare the host series prior to carbonation. The study of the $PrTiFe_{11-x}Co_x$ series is then the preliminary step to that of carbides $PrTiFe_{11-x}Co_xC_y$.

Herein, we report structure, Mössbauer effect study and Curie temperature measurements of the precited series for which no attempt had been made up to now to prepare either the $PrTiFe_{11-x}Co_x$ or the carbides. Mössbauer spectrometry appears as a complementary tool to x-ray investigation be-

cause it is suitable, as local atomic probe, to distinguish the iron environment in the various crystallographic sites and, hence, the cobalt location and the carbon perturbation.

II. EXPERIMENT

The polycrystalline $PrTiFe_{11-x}Co_x$ ingots ($x \leqslant 3$) were prepared by induction melting from appropriate amounts of 99.9% purity Pr, Fe, Ti and Co under a highly purified Ar atmosphere. Their homogeneity was insured with ten times consecutive melting. The as-cast alloys wrapped in tantalum foil and sealed in silica tubes under a vacuum of 5×10^{-7} Torr were annealed six days at 1373 K and water quenched. Prior to carbonation, the sample composition was checked by electron microprobe analysis with an accuracy of $\pm 5\%$. The carbides $PrTiFe_{11-x}Co_xC_y$ with $y=1$ were synthesized using a solid-solid reaction as described previously.[16] The carbon transfer into the $I4/mmm$ structure was monitored after reacting the $PrTiFe_{11-x}Co_x$ compound ground to 50 μm powder size with an appropriate over weight of $C_{14}H_{10}$ powders, the same for all x content, in order to obtain the maximum possible carbon insertion of one carbon atom per unit formula. At temperature above 673 K, it was shown that the carbon insertion is immediate. Mg chips inside the reacting tube absorb the overpressure of H. However to insure a good homogeneity of the carbon distribution, the samples were annealed 48 h at 750 K.

The x-ray diffraction (XRD) patterns were recorded by means of a Bruker diffractometer mounted with the Bragg-Brentano geometry and automatic divergence slit, using the Cu $K\alpha$ radiation. The unit cell parameters were measured with Si as standard ($a=5.4308$ Å). The counting rate was 22 s per scanning step and step size of 0.04°. The data treatment was carried out by a Rietveld refinement[17,18] as implemented in the FULLPROF computer code[20,19] with the assumption of a peak line profile of Thompson-Cox-Hastings allowing multiple phase refinement of each of the coexisting phases. The goodness-of-fit indicators R_B and χ^2 are calculated as usual and described earlier.[21,22] The Curie temperature T_C measurements were performed with a MANICS differential sample magnetometer under an applied field of 1000 Oe with around 10 mg sample sealed under vacuum.

The Mössbauer spectra were obtained between 77 and 293 K on a constant-acceleration spectrometer in transmission geometry. The parabolic distortion was canceled by working in the mirror image mode and the small resulting linear drift of the baseline was corrected. The γ-ray source was 50 mCi cobalt-57 embedded in rhodium matrix. The absorbers contained around 15 mg/cm^2 of natural iron. Hyperfine fields are quoted relative to a high purity metallic α-iron foil absorber at room temperature used to calibrate the spectrometer. This reference had a full-width at half maximum of 0.25 mm/s for the external peaks. The folded Mössbauer spectra presented herein contain 512 channels. The fitting procedure will be explained below. The estimated errors are at most ± 0.1 T for hyperfine fields H_{HF} and ± 0.005 mm/s for isomer shifts δ and quadrupole shifts 2ε.

TABLE I. Microprobe analysis results.

Nominal composition		$x=0$	$x=1.5$	$x=2$	$x=3$
Experimental composition	Pr	1.00	1.00	1.00	1.00
	Fe	10.96	9.42	8.89	7.95
	Co	0	1.52	2.07	2.95
	Ti	1.04	1.06	1.04	1.10

III. RESULTS AND DISCUSSION

A. Microprobe analysis

The electron microprobe images, versus Co content of the alloys $PrTiFe_{11-x}Co_x$, have shown some minor precipitates identified as αFe-(Ti,Co) and Fe_2Ti, imbedded in a matrix corresponding to the major phase 1:12. The chemical composition of the matrix is reported in Table I for $x=0$, 1.5, 2, and 3. It appears from these results that the nominal composition is representative of the experimental ratio Fe/Co and Ti/Fe.

B. X-ray diffraction

1. $PrTiFe_{11-x}Co_x$

The x-ray diffraction diagrams of the $PrTiFe_{11-x}Co_x$ annealed at 1373 K, reveal the presence of the main phase with the tetragonal $ThMn_{12}$ structure with space group $I4/mmm$, and weak extra lines which belong to αFe-(Ti,Co), Fe_2Ti (for $x=0$ and 0.5). As well known in the $RFe_{11}Ti$ alloys, Ti occupies the $8i$ site.[23] For the Rietveld fit, the Co atoms, which cannot be discerned by x-ray from Fe, have been located statistically in $8i$, $8j$, $8f$ sites according to the nominal composition of each sample in a first approach. However, as justified by the Mössbauer spectra analysis given below, the Rietveld fits were finally performed with Co distributed in $8f$ sites.

The calculated patterns along with the observed ones are presented on Fig. 1(a) for $x=1.5$ as an example. The atomic positions and unit cell parameters obtained from the Rietveld fit are given in Table II. The substitution of Co for Fe induces a decrease of both parameters a and c, however, the c/a ratio remains constant and equal to 0.557 for all x (Fig. 2). The small size difference between Fe and Co radii cannot alone explain such reduction. The magnetic coupling energy between each sublattice R and M combined with an electronic effect due to the additional Co $3d$ electron should play a role. In the case of $SmTiFe_{11-x}Co_x$ alloys ($x \leqslant 2$) (Refs. 22 and 24), for which the crystalline field favors a ferromagnetic coupling between R and T sublattices along c, the a parameter is insensitive to the Co substitution while c decreases weakly with x. Nevertheless for $PrTiFe_{11-x}Co_x$ which do not show an axial magnetic anisotropy up to $x=3$, both parameters decrease. Their monotonous behavior suggests a unique mode of Co substitution for Fe up to $x=3$.

The volume ratio of the extra phases deduced from the Rietveld fits corroborates the results from the microprobe-

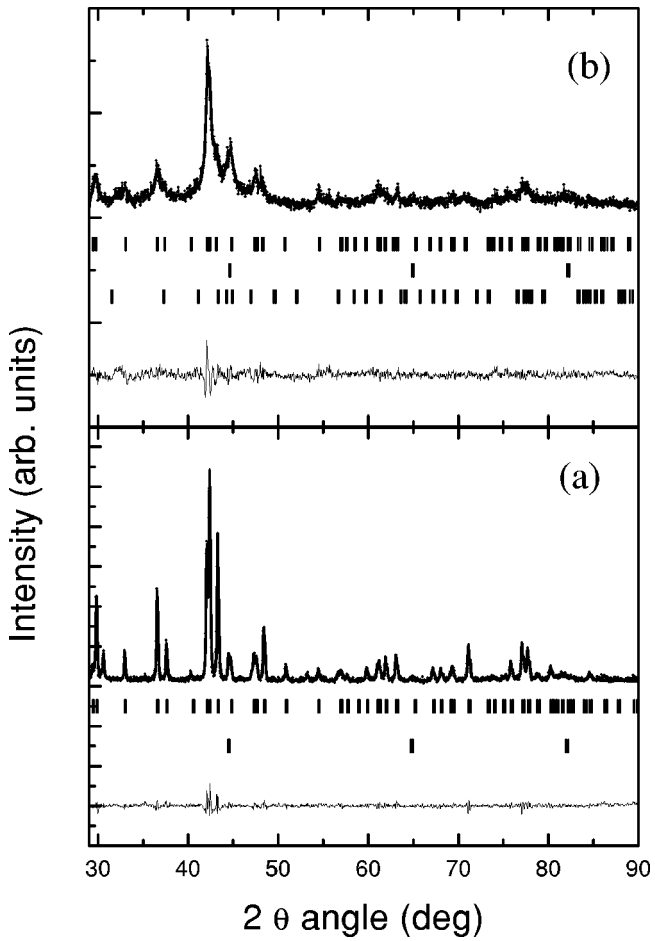

FIG. 1. Rietveld analysis for (a) $PrTiFe_{9.5}Co_{1.5}$ and (b) $PrTiFe_{9.5}Co_{1.5}C$. The set of ticks refer, respectively, to (a) the $ThMn_{12}$ phase and αFe-(Ti,Co), and (b) $ThMn_{12}$ phase, αFe-(Ti,Co), and Fe_2Ti.

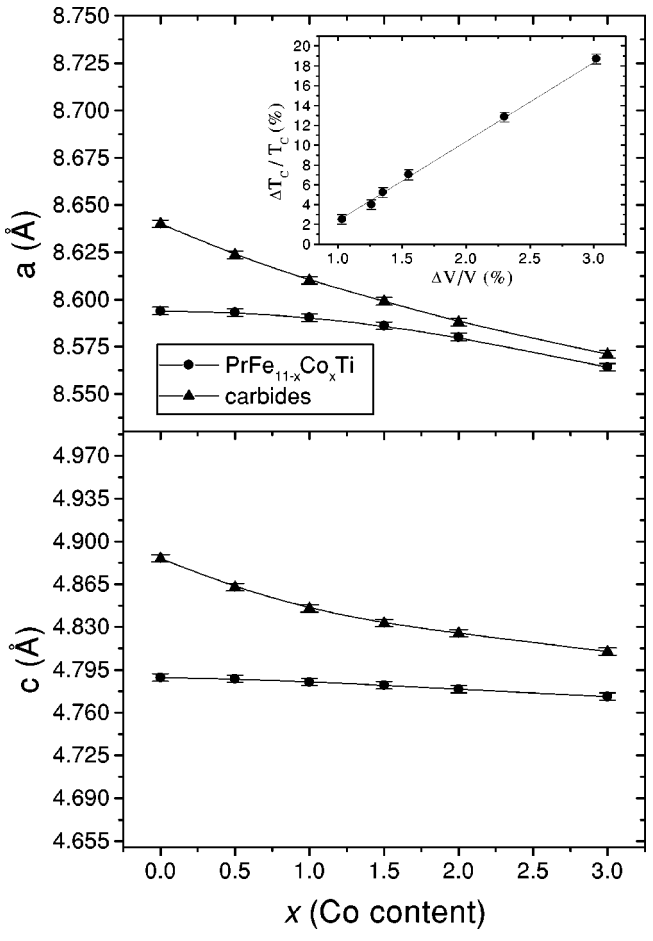

FIG. 2. Unit cell parameters vs Co content of $PrTiFe_{11-x}Co_x$ and $PrTiFe_{11-x}Co_xC$. $\Delta T_C/T_C$ vs $\Delta V/V$ (inset). Solid line is a guide for eyes.

analysis. Their total amount is never higher than 7%. It decreases down to 3.8% for $x=3$. The substitution of Co reduces the precipitation of small αFe-(Ti,Co) contents which might result from the peritectic formation reaction.

2. $PrTiFe_{11-x}Co_xC$

The crystalline qualilty of the samples annealed at 750 K allows a good determination of the unit cell parameters (Table II). The carbides $PrTiFe_{11-x}Co_xC$ clearly show an an-

TABLE II. a, c cell parameters and R_B, χ^2 factor from Rietveld fit for $PrTiFe_{11-x}Co_x$ and their carbides.

Compound		$x=0$	$x=0.5$	$x=1$	$x=1.5$	$x=2$	$x=3$
$PrTiFe_{11-x}Co_x$	a(Å)	8.594	8.592	8.590	8.588	8.582	8.564
	c(Å)	4.789	4.787	4.786	4.782	4.779	4.773
	R_B	5.38	5.81	5.01	5.39	3.47	4.55
	χ^2	1.54	2.01	1.37	1.47	1.18	1.35
	$X\{8i\}$	0.361	0.359	0.359	0.359	0.358	0.358
	$X\{8j\}$	0.275	0.272	0.274	0.274	0.273	0.273
	T_C(K)	550	618	670	705	740	785
$PrTiFe_{11-x}Co_xC$	a(Å)	8.640	8.624	8.602	8.599	8.593	8.572
	c(Å)	4.885	4.863	4.839	4.833	4.829	4.813
	R_B	4.64	5.78	5.08	5.36	4.93	5.65
	χ^2	1.74	1.67	1.49	1.47	1.22	1.37
	$X\{8i\}$	0.363	0.363	0.363	0.362	0.364	0.364
	$X\{8j\}$	0.272	0.272	0.272	0.270	0.270	0.271
	T_C(K)	656	691	726	757	776	818

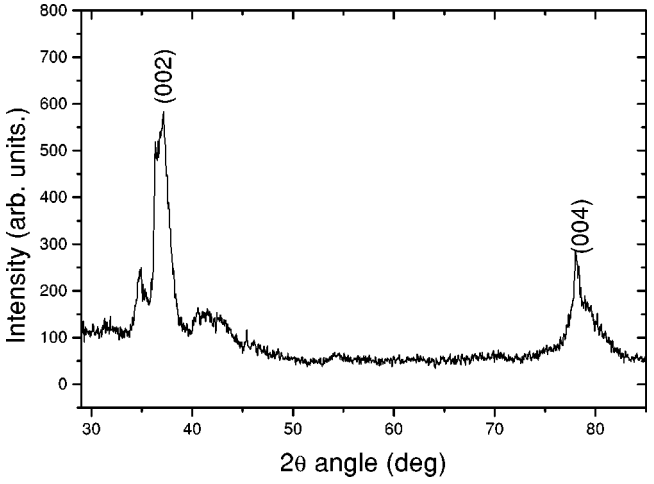

FIG. 3. XRD pattern of aligned carbide for $x=1.5$, as an example

isotropic unit cell expansion with respect to their homologous $PrTiFe_{11-x}Co_x$. The calculated and experimental patterns are shown in Fig. 1(b) for $x=1.5$ as an example. The results of the Rietveld refinement are listed in Table II.

For $x=0$, $\Delta a/a$ and $\Delta c/c$ are respectively equal to 0.5 and 2.03% more than for the nitride investigated previously.[12] These values lead to a volume increase similar to the maximum uptake of one carbon per unit formula observed in the $R(Fe_{12-x}M_x)$ series stabilized by $M=$Mo (Ref. 25). With Co content, the volume expansion is reduced monotonically to 1.8% for $x=3$ but this evolution is mainly associated to a c increase. The carbon insertion induces the expansion of the Pr-Fe($8i$)-Fe($8i$)-Pr chains along the a axis via the carbon $2p$ and iron $3d$ electrons while the c axis increase is connected to the more important elongation of the bi-pyramid Pr($2a$)-Fe($8j$) which delimits the interstitial carbon site $2b$ via the carbon ($2p$) and Pr ($5d$,$6s$) electrons.

The unit cell parameters measured for $x=2$ with a nominal carbon content equal to 0.5 atom per unit formula leads to a volume increase equal to half of the increase measured for the saturated sample with one atom per unit formula. We can therefore assess that the whole series corresponds to the maximum carbon uptake of one carbon, as all samples were prepared in the same conditions.

X-ray diffractometry was also performed on powder samples of carbides previously magnetically aligned under an external field of 0.7 T. It reveals that the magnetization is aligned along the c axis of the tetragonal structure in $PrTiFe_{11-x}Co_xC$. An example of such diffraction pattern is given in Fig. 3. Some grains may be misoriented, not strictly monodomain and thus can contribute to some Bragg peaks other than ($00l$). Nevertheless, both the growth of the ($00l$) reflections [(002) and (004)] and the disappearance of the ($hk0$) reflections give evidence for a preferential orientation of the basal plane along the reflecting surface. Under carbonation the magnetic anisotropy turns from planar to uniaxial with Co content up to $x=3$, at room temperature as observed for carbon uptake per unit formula equal to one atom.

C. Curie temperature measurements

The Curie temperature of the $PrTiFe_{11-x}Co_x$ alloys increases from 550 K for $x=0$ to 785 K for $x=3$, while a small decrease of the Fe-Fe distances, at most equal to 0.3% is observed. This T_C raise reflects the enhancement of the Fe-Fe interactions and can be explained by electronic effects. The Fe weak ferromagnetic character is progressively modified into strong ferromagnetism upon the filling of the d band with the additional Co electron.

Upon carbonation, the T_C values are also enhanced, compared to the $PrTiFe_{11-x}Co_x$ alloys (Table II). In that case, the unit cell expansion induces a strengthening of the Fe-Fe interactions due to the increase of the Fe-Fe distances. The T_C increase, $\Delta T_C/T_C$, equal for $x=0$ to 19.4% is, however, reduced to 4.2% for $x=3$. One must outline that all interatomic distances in the $PrTiFe_{11-x}Co_x$ alloys, whatever x, are higher than the critical distance of 2.39 Å, limit with negative magnetic interactions, except the interatomic distance d_{8f-8f} equal to 2.39 Å. This distance augments to 2.44 Å for $PrTiFe_{11}C$. For $x=3$, it is only increased to 2.41 Å. A linear correlation is observed between $\Delta T_C/T_C$ and the volume expansion $\Delta V/V$ related to the initial host lattice [Fig. 2 (inset)].

The enhancement of the Curie temperatures is the result of two combined effects: filling of the d band by the Co electrons and Fe-Fe distances increase. For saturated carbon alloys, with Co increasing, it seems that the electronic effect dominates progressively the volume effect to rule the T_C evolution.

D. Mössbauer spectra

For simplicity, the Mössbauer spectral analysis has been performed first on the $PrTiFe_{11-x}Co_x$ alloys. Afterwards, the effect of carbon should be more easily understood. However, for both series the same general considerations are available.

We must outline that the atomic arrangements are rather complex due, on the one hand, to the existence of three crystallographic sites and, on the other hand, to the statistical distribution of Ti and Co. Consequently, the experimental spectra result from the superposition of numerous sextets. Various sets of hyperfine parameters might lead to a good reproduction of the data but the choice of the solution is dependent on consistent physical models supported by other techniques or justified by pertinent theoretical considerations.

We have based the Mössbauer spectra analysis upon two criteria: the count of the different iron neighboring according to the binomial law, the assignment of the hyperfine parameter sets δ, H, and 2ϵ of an individual sextet to its right crystallographic site, in agreement with the relationship between isomer shift and Wigner-Seitz cell (WSC) volumes: the larger the WSC volume, the larger the isomer shift δ. The WSC volumes have been calculated by means of Dirichlet domains and coordination polyhedra for each crystallographic family. The radius values of 1.82, 1.26, 1.25, and 1.47 Å have been used respectively for Pr, Fe, Co, and Ti. However, for C, the twelve coordinated atomic radius of 0.92 Å is inconsistent with the $2b$ octahedral site size for all x

TABLE III. Near-neighbor environments and WSC volumes (Å^3) in $PrTiFe_{10}Co$ and in $PrTiFe_{10}CoC$ as an example.

Site	$Pr\{2a\}$	Fe/Ti$\{8i\}$	Fe$\{8j\}$	Fe/Co$\{8f\}$	C$\{2b\}$	Iron near neighbors	WSC volume $PrTiFe_{10}Co$	WSC volume $PrTiFe_{10}CoC$
Pr$\{2a\}$	0	4	8	8	2	17	23.22	25.30
Fe/Ti$\{8i\}$	1	5	4	4	0	10.75	12.10	12.79
Fe$\{8j\}$	2	4	2	4	1	8	11.54	11.95
Fe/Co$\{8f\}$	2	4	4	2	0	8.5	10.51	11.46
C$\{2b\}$	2	0	4	0	0	4		2.68

content. The site diameter which varies from 1.45 Å for $x=0$ down to 1.40 Å for $x=3$ is more in agreement with the covalent radius value of 0.77 Å generally given for C. Hence, we have used the carbon radius value of 0.73 Å for $x=0$ and 0.70 Å for $x=3$, for the calculation of the WSC volumes reported in Table III, within the size limits calculated from the measured octahedral $2b$ site size. The following sequence of the WSC volumes $8i>8j>8f$, whatever x, is obeyed for the $PrTiFe_{11-x}Co_x$ and the carbides. Moreover for the fits, we have taken into consideration the weak extra iron-based phases observed by XRD that might be not neglected as their Lamb-Mössbauer factor is larger than for the *R*-Fe phase.

Four assumptions have been made: (i) The $8i$ sites are those occupied by the stabilizing transition elements of the 1:12 structure.[26] They must obey steric and electronic criteria. The atomic radius of these elements must be greater than Fe radius and the number of their $3d-4s$ electrons smaller.[27] It results that the Co substitution in $8i$ site has been excluded. (ii) Co atom occupies $8f$ sites according to previous Mössbauer spectroscopy results on $Y(Fe,Co)_{11}Ti$ (Ref. 28) and neutron diffraction measurements on $Nd(FeTiCo)_{12}$ (Ref. 29). (iii) The Lamb-Mössbauer factors are equal for all sites $8i$, $8j$, $8f$ of the 1:12 structure. (iv) As no crystallographic texture was observed, the relative intensity of each sextet line was taken in the ratio 3:2:1 of random powders.

Consequently, in a first step we have calculated the relative abundances of the Fe families in the various crystallographic sites $8i$, $8j$, and $8f$ with the assumption of Ti in $8i$ site, Co in $8f$ site with the multinomial law. These assertions will be justified below by the coherency of the hyperfine parameter evolution vs x and temperature. All along the fitting process, these abundances were maintained as fixed parameters, they were normalized after neglecting those lower than 2%. All other parameters viz. δ, H_{HF}, and 2ϵ were free. In the second step of the refinement, the deduced averaged isomer shift values have been assigned to each site of the $8i$, $8j$, $8f$ families according to the WSC volume relationship. Finally, in the last step of the fit all hyperfine parameters were free.

1. $PrTiFe_{11-x}Co_x$

Figure 4 shows the Mössbauer spectra at room temperature for all x content and Fig. 5 reports the spectra of $PrTiFe_{10}Co$ at various temperatures between 77 and 293 K. For $x=0$, according to the number k of Ti neighbors, a total of nine sextets has been used to simulate the $8i$, $8j$, $8f$ sites. The spectra of the substituted samples (for $x>0$) were explained with the same approach but, the combined effects of l Co neighbors were considered. As an example, to keep a physical meaning to the various abundances, k was limited to 2 and l to 3 for $x=2$. The set of hyperfine parameters resulting from such a fit are reported in Table IV for $x=1.5$ at 77 K.

The isomer shift behavior with Co content at 293 K is reported on Fig. 6(a) At all temperatures, for a given x value, the relation $\delta\{8i\}>\delta\{8j\}>\delta\{8f\}$ is always obeyed, according to our assumption derived from the WSC volumes. The mean isomer shift of the $8i$ and $8j$ atoms increase upon Co substitution, while it remains quasiconstant for the $8f$ atoms.

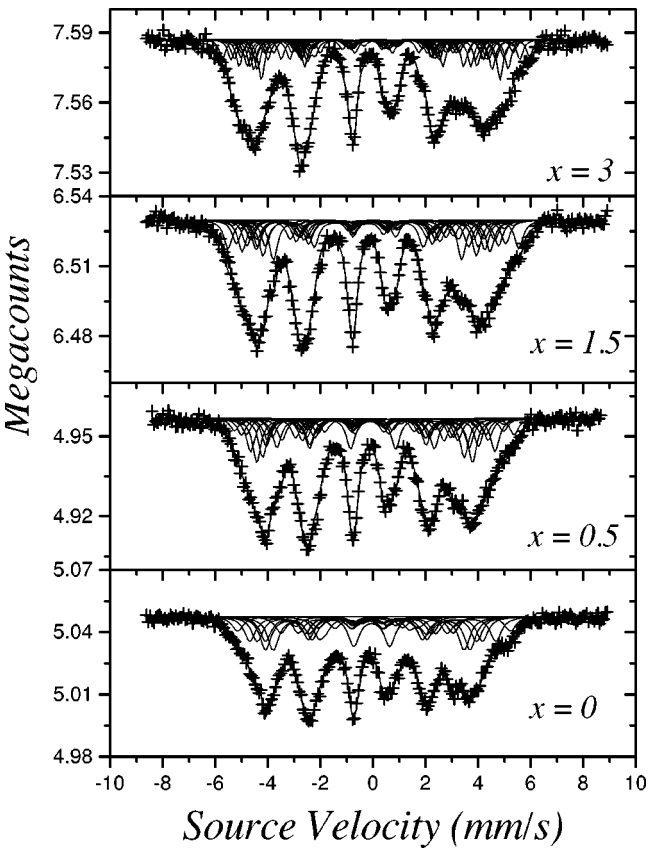

FIG. 4. The 293 K Mössbauer spectra and their decomposition (see text) of $PrTiFe_{11-x}Co_x$.

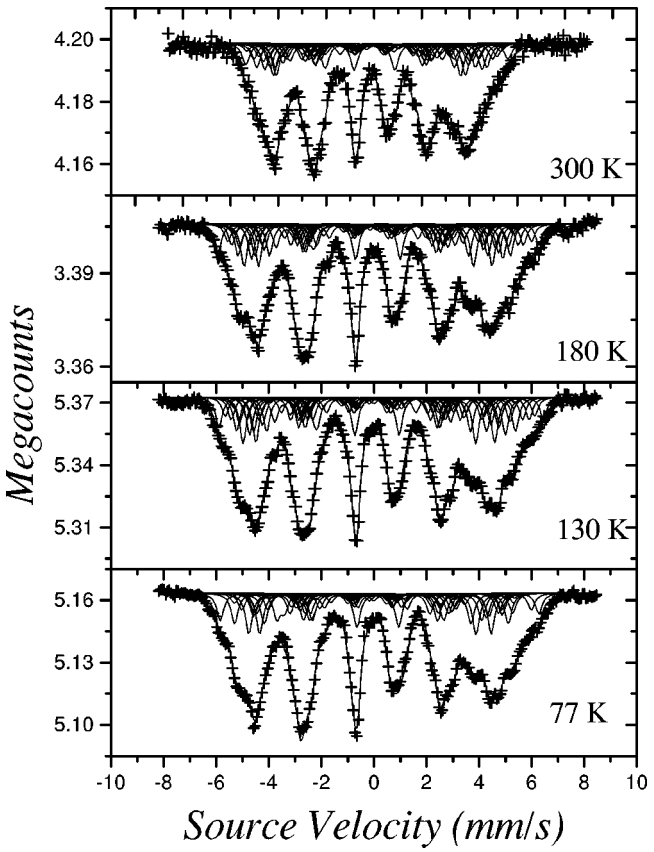

FIG. 5. Mössbauer spectra and their decomposition (see text) of $PrTiFe_{10}Co$ obtained at indicated temperature.

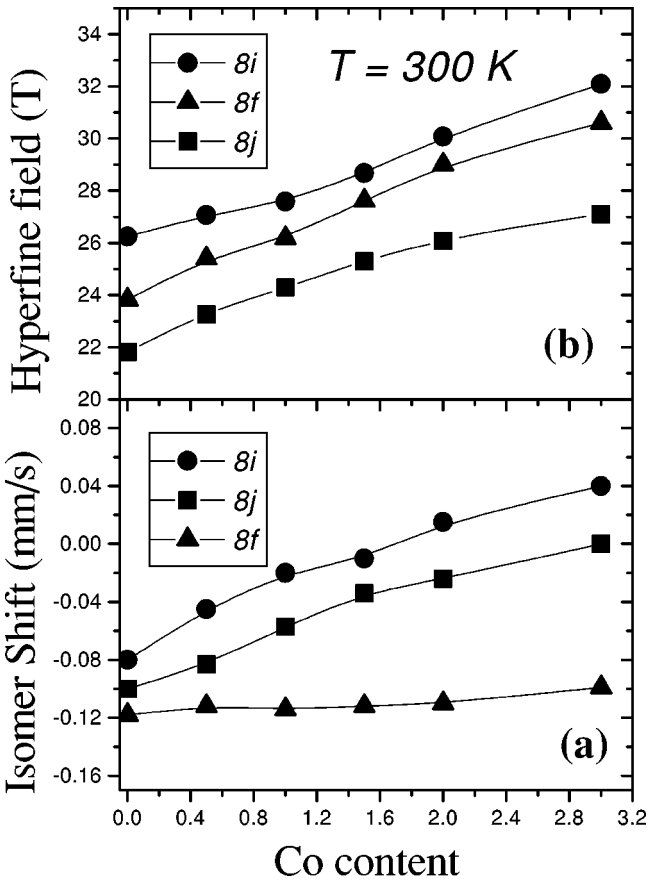

FIG. 6. The compositional dependence of (a) the isomer shifts and (b) the hyperfine fields at 293 K for $PrTiFe_{11-x}Co_x$. Solid line is a guide for eyes.

This result can be understood in terms of the preferential Co atom occupation. The WSC volume reduction which might contribute to an increase in the *s*-electron density at the Fe nuclei is widely balanced by the enhancement of the *d* electron density brought by Co which, in turn, gives rise to a reduction of the *s* electron density at the Fe nuclei. The additional Co *d* electron favors the shielding of the 4*s* electrons. It results an increase in the isomer shift for the Fe sites having Co first neighbors and weaker effect for the site where Fe/Co are located. The 8*i* and 8*j* Fe sites have four

TABLE IV. Mössbauer hyperfine parameter for $PrTiFe_{9.5}Co_{1.5}C_y$ ($x=1.5$) at 77 and 293 K. Hyperfine field, H_{HF}; Isomer shift, δ; relative area, *S*, and quadrupole interaction, 2ε.

	y	T(K)	$8i_{11}$	$8i_{12}$	$8i_{21}$	$\langle 8i\rangle$	$8j_{01}$	$8j_{02}$	$8j_{11}$	$8j_{12}$	$8j_{21}$	$\langle 8j\rangle$	$8f_{00}$	$8f_{01}$	$8f_{10}$	$8f_{11}$	$\langle 8f\rangle$
$H_{HF}(T)$	0	77	33.7	31.8	28.1	31.5	27.6	28.5	25.6	26.2	24.4	26.6	31.2	29.7	27.8	28.2	29.8
		293	28.6	29.3	28.0	28.7	27.0	28.2	24.0	24.5	27.0	25.3	28.6	27.9	27.0	26.2	27.6
	1	77	34.3	35.1	30.2	33.5	32.5	32.6	27.5	31.1	22.2	29.5	32.1	33.9	24.5	28.9	30.6
		293	31.0	32.0	30.5	31.2	28.0	28.5	25.6	26.4	23.6	26.5	29.6	31.1	29.1	26.7	29.6
δ(mm/s)	0	77	0.098	0.068	0.045	0.072	0.041	0.054	0.023	0.028	0.018	0.033	−0.012	−0.011	−0.058	−0.068	−0.021
		293	0.002	−0.011	−0.032	−0.010	−0.012	−0.012	−0.023	−0.121	−0.119	−0.030	−0.099	−0.111	−0.129	−0.166	−0.112
	1	77	0.212	0.169	0.101	0.165	0.084	0.089	0.062	0.069	0.058	0.069	0.019	−0.011	−0.012	−0.031	−0.003
		293	0.032	0.021	0.011	0.020	0.021	0.029	−0.045	−0.065	−0.091	−0.010	−0.016	−0.019	−0.064	−0.052	−0.032
2ε(mm/s)	0	77	0.16	0.10	0.14		0.10	0.10	0.12	0.12	0.10		0.10	0.10	0.00	0.05	
		293	0.04	0.03	0.14		0.07	0.07	0.10	0.10	0.13		0.06	0.05	−0.01	0.07	
	1	77	0.13	0.10	0.14		0.10	0.11	0.12	0.13	0.12		0.10	0.10	0.00	0.05	
		293	0.12	0.10	0.16		0.10	0.10	0.12	0.12	0.18		0.10	0.10	0.00	0.08	
S(%)			8.8	7.9	5.9		9.1	8.2	12.1	10.9	6.1		6.1	7.3	8.1	9.7	

adjacent $8f$ neighbors while the $8f$ site atoms have only two. In contrast, if $8f$-atom neighboring is poorly affected by the Co substitution, the *s* charge density is then not modified. A weak change is observed for the $\delta\{8f\}$. The difference for the $8f$ site behavior then corroborates the preferential occupation of Co atoms on this site. This later result is in agreement with the results obtained for $YFe_{11-x}Co_xTi$ (Ref. 28) and $SmFe_{11-x}Co_xTi$ (Ref. 22).

The monotonous H_{HF} variation with *x*, and *T* for a given *x*, corroborates the validity of the field assignment. As reported versus Co content at room temperature on Fig. 6(b), the weighted average hyperfine field increases with *x* in connection with the observed and expected increase of the Curie temperature upon Co substitution. In the 1:12 structure, undoubtedly, the $8i$ site with the highest number of Fe neighbors, so far, is expected to show the highest H_{HF} (Table IV). However, it appears, that $H_{HF}\{8f\}$ is always larger than $H_{HF}\{8j\}$. This hyperfine magnetic field sequence which results from the assignment of the hyperfine parameter sets based on the correlation between δ and H_{HF} is in agreement with the sequence of the magnetic moments determined by neutron diffraction data on $YTi(Fe,Co)_{11}$ (Ref. 30) and Mössbauer study on $RTi(Fe,Co)_{11}$ $R=Y$, Dy and Er (Ref. 31). However, our hyperfine magnetic field sequence does not follow other previous analysis[32–34] supported by the local magnetic moment μ sequence measured by neutron diffraction on $Y(Ti,Fe)_{12}$ (Ref. 35), $\mu\{8i\}>\mu\{8j\}>\mu\{8f\}$.

The main contribution to the hyperfine field, i.e., the Fermi contact term H_{FC}, arises from the interaction between the Fe nucleus magnetic moment and the magnetic field due to its own *s* electrons. It originates from two opposite terms: the negative core-electron polarization field H_{CE} and the positive $4s$ conduction-electron polarization field H_{4s}. H_{CE} results from the difference in spin-up and spin-down charge densities in *s* shell produced by the partial filling of the *d* band and arises directly from the local *d* moment. Within the μ sequence given above for $Y(Ti,Fe)_{12}$, it might be proposed that this negative contribution, proportional to the *d* moment, might be partially balanced by the conduction electron positive term H_{4s} arising from changes induced by the *d* moment distribution on the Fe site. This compensation might be more pronounced for $8j$ than for $8f$ Fe atoms and would lead to the observed sequence $H_{HF}\{8f\}>H_{HF}\{8j\}$.

The change with increasing Co content is due to the known effect of transition metal at the right side of Fe, even though the local moment of the substituting atom is less than that of Fe. Upon substitution, the additional Co electron contributes to the asymmetric filling of the *d* band and might enhance the negative core-electron polarization term. It then follows that the mean hyperfine field increases. The same trend for each individual site is observed within the same scheme $H_{HF}\{8f\}>H_{HF}\{8j\}$.

2. $PrTiFe_{11-x}Co_xC$

The Mössbauer spectra of $PrTiFe_{11-x}Co_xC$ were measured between 77 and 293 K. The results at 77 K are shown as an example in Fig. 7 for various cobalt contents. The linewidth remains the same than for $PrTiFe_{11-x}Co_x$, suggesting that the possible disorder introduced by carbon insertion in the lattice is of second order, the statistical arrangement of Ti and Co being the main cause of the line broadening.

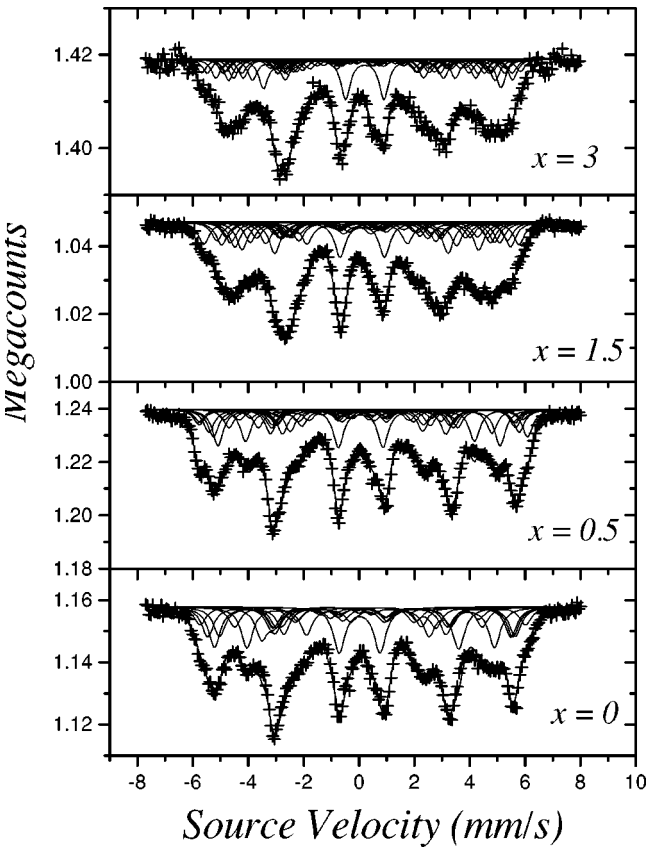

FIG. 7. The 77 K Mössbauer spectra and their decomposition (see text) of $PrTiFe_{11-x}Co_xC$.

The compositional dependence of the isomer shift and the hyperfine magnetic field, for the three iron sites, are shown, respectively, in Figs. 8(a) and 8(b). The isomer shift for the different iron sites in the carbides are in good agreement with those obtained for $PrTiFe_{11-x}Co_x$ and correlate with their WSC volumes, as described above. The isomer shift in carbides shows similar temperature dependence.

The isomer shift is affected by the presence of interstitial element. Going from $PrTiFe_{11-x}Co_x$ to their carbides we have noticed an increase of the isomer shift at the Fe nuclei. The increase of δ reflects the decrease of electron density with carbon insertion. It indicates a charge transfer from the rare-earth $6s$ orbital into the carbon atoms combined with the effect of the volume expansion which is quite significant. Similar trends on the isomer shift are observed upon nitrogen or carbon insertion as reported in Ref. 36. This means that, whatever the interstitial element in the $ThMn_{12}$ crystal structure, a modification of the rare-earth $6s$ orbital is observed. This is not surprising because the interstitial elements act as first neighbors of the rare earth. In addition the short bonds observed between Pr and the interstitial witness to hybridization. The assignment of the $8i$, $8j$ and $8f$ site isomer shifts in the carbides is also in agreement with their relative WSC

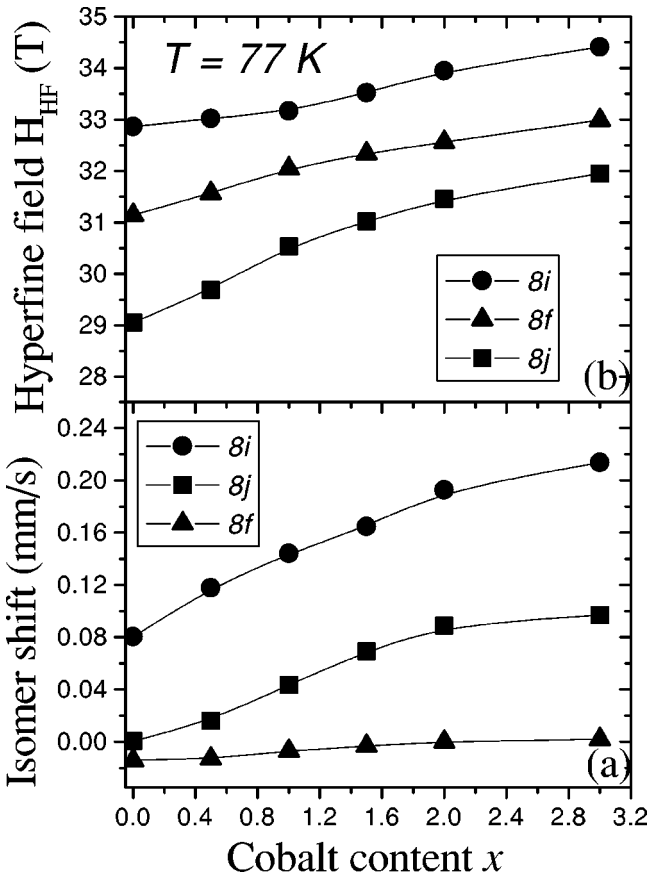

FIG. 8. The compositional dependence of (a) the isomer shifts and (b) the hyperfine fields at 77 K for $PrTiFe_{11-x}Co_xC$. Solid line is a guide for eyes.

volumes. As it is shown in Fig. 8(a), the isomer shift sequence is $8i>8j>8f$.

Upon carbonation, the general increase in the isomer shift results from the unit cell expansion which decreases the *s*-electron density at the iron nucleus. This effect is best illustrated with the linear relation between the weighted average isomer shift and the unit cell volume, which indicates that the unit cell expansion is responsible primarily for the increase of the isomer shift. A plot of the weighted average isomer shift versus the unit cell volume reveals a perfectly linear correlation $\delta=\alpha V+\beta$, where $\alpha=9.17\times10^{-3}$ (mm/s)/Å^3 and $\beta=-3.34$ mm/s.

This overall expansion of the lattice results in the well-known volume effect on the weighted average isomer shift. The decrease of the electron density at the iron nucleus produces an increase in the observed weighted isomer shift $\Delta\delta$ of 0.102 mm/s. This value agrees with the increase of 0.1 mm/s reported by Hu *et al.*,[37] who prefer to estimate the volume effect on the isomer shift by calculating $\Delta\delta/\Delta\ln V$. Phenomenologically, the effect of volume change on the isomer shift of iron is well established $\Delta\delta/\Delta(\ln V)=1.3$ mm/s (Ref. 38), and this gives a yardstick by which additional influences of chemical bonding may be assessed. Taking the relative volume expansion values $\Delta V/V=\Delta\ln V=3.09\%$, we found that $\Delta\delta/\Delta\ln V$ on carbonation is 3.2 mm/s. This is larger than the value for $R_2Fe_{17}N_x$ ($\Delta\delta/\Delta\ln V=1.7$ mm/s Ref. 37) and better agrees with that for $R(Fe_{11}Ti)N_x$ value ($\Delta\delta/\Delta\ln V=2.6$ mm/s Ref. 6): it is consequently suggested that the interband electron transfer on carbonation in $PrTiFe_{11-x}Co_x$ is stronger than in nitrides of the 2:17 series.

The effect of carbonation on the isomer shift may be discussed on the basis of either the weighted average isomer shift or the individual site isomer shifts. Upon carbonation, the unit cell volume expands, and hence the WSC volume of each site increases. In order to understand the effect of carbonation on the isomer shift of an individual iron site, both the volume increase upon carbonation and the presence of a near-neighbor carbon atom must be considered. The $8i$ and $8f$ sites have no carbon near neighbors and, hence, we expect to observe only the influence of the volume increase on the isomer shift. For the $8j$ site with one carbon near neighbor, a combined volume increase and near-neighbor carbon influence on the isomer shift is expected. For the $8i$, $8f$, and $8j$ sites the isomer shift increase ($\Delta\delta$), and Wigner-Seitz cell volume increase ($\Delta\ln V$), and the ratio ($\Delta\delta/\Delta\ln V$) are, respectively, 0.098, 0.092, and 0.116 mm/s, 0.049, 0.128, and 0.086, 2.01, 0.72, and 1.35 mm/s. The $8i$ and $8f$ sites show similar values of the isomer shift increase, which are due only to lattice expansion of the Wigner-Seitz cell volume. For the $8j$ site, the isomer shift increase of 0.116 mm/s is the largest and may be attributed to both effects, the carbon near neighbor and the lattice expansion of the Wigner-Seitz cell volume.

The magnetic hyperfine fields for each site in the carbides are given in Table IV, for $x=1.5$, and are shown as a function of cobalt content in Fig. 8(b). The sequence of hyperfine fields does not agree with the sequence suggested by Yang *et al.*[35]

It can be seen from Table IV that there is an increase in the H_{HF} at all iron sites on carbonation which can be discussed on the basis of either the magnetovolume and the chemical effects. The first effect causes an increase of magnetic moment as a result of lattice expansion and a consequent $3d$ band narrowing. The second effect is due to the difference in the electronegativity of iron and carbon and causes transfer of charges from the *s* and *p* bands of carbon to the $3d$ band of nearest iron. Heine[39] has calculated that in transition-metal-rich compounds, the width of the $3d$ band is inversely proportional to the fifth power of the lattice parameter. The narrowing of the $3d$ band induces more localization of the $3d$ electrons and a concomitant moment enhancement. Dong, Yang and Yang[40] have observed an increase in the magnetic moment of $RTiFe_{11}$ on nitrogenation, which is also attributed to the band narrowing effect.

As it is shown in Figs. 6(b) and 8(b) the introduction of cobalt into the Fe sublattice causes an increase in the value of hyperfine field for all crystal sites. This behavior is observed at all temperatures from 77 to 293 K. Upon carbonation, the $8j$, $8i$, and $8f$ hyperfine fields increase by around 1.1, 2.8, and 3.7 T, in relation with the increase of magnetization and Curie temperature. The minor increase of $8j$ hyperfine field might be due to the presence of one carbon as nearest neighbor. If a conversion factor of $15T/\mu_B$ is used at room temperature the $8i$, $8j$, and $8f$ site magnetic moments, for $x=0$, are 1.74, 1.45, 1.59 μ_B for $PrTiFe_{11}$ and 1.93, 1.53,

1.83 μ_B for their carbides. Upon carbon insertion, the $8f$ site shows the highest hyperfine field increase, which can be correlated to the increase of the Fe-Fe interatomic distance, hence the WSC volume of f.

The increase of 12% in average hyperfine fields, from 23.8 to 26.8 T, at room temperature after carbonation derives from the large increase of Curie temperature, from about 550 K for $PrTiFe_{11}$ to 656 K for carbide Table II. At 77 K there is approximately a same change of the average hyperfine field after carbonation, about 3.3 T (12%) which is smaller than the increase of 13.4% found in the case of $NdFe_{11}TiN_{0.8}$ (Ref. 41). All the quadrupole shift values are small and temperature independent within the experimental accuracy.

IV. CONCLUSION

The $PrTiFe_{11-x}Co_x$ host alloys ($x \leqslant 3$) have been successfully prepared by melting and subsequent annealing. The carbon transfer was performed by means of a solid-solid reaction with $C_{14}H_{10}$ powders which allows the maximum carbon insertion of one atom per unit formula. The Rietveld refinement have shown that all compounds are $ThMn_{12}$-type. The unit cell parameter variation with cobalt content, measured against the standard Bragg reflection of Si mixed with the sample, exhibits a small decrease of both a and c parameters, for the $PrTiFe_{11-x}Co_x$ alloys while upon carbonation, a significantly anisotropic unit cell expansion is observed. X-ray diffraction analysis of magnetic field aligned carbide powders has revealed that the magnetic anisotropy turns from planar to uniaxial up to $x=3$. Change in electronic structure upon cobalt substitution and dilatation of the crystal lattice upon carbonation are responsible for the Curie temperature raise. For the carbides, a linear relationship between the volume expansion and the Curie temperature increase can be given.

The Mössbauer spectra collected between 77 and 293 K for both series have been analyzed taking into account the statistical distribution of Ti in $8i$ sites. The hyperfine parameter set attribution has been performed according to the correlation between Wigner-Seitz cell volumes and isomer shift δ. At all temperatures, for a given x value, it results the following sequence $\delta\{8i\} > \delta\{8j\} > \delta\{8f\}$. This assignment induces the hyperfine field correlation $H_{HF}\{8i\} > H_{HF}\{8f\} > H_{HF}\{8j\}$ which can be understood on the basis of the competition between the negative core-electron polarization field and the positive conduction-electron polarization field. In the $PrTiFe_{11-x}Co_x$ alloys, upon Co substitution, the $\delta\{8i\}$ and $\delta\{8j\}$ increase is explained by the perturbation brought by Co neighbors. The reduction of the s electron density at the corresponding Fe nuclei is due to the shielding of the $4s$ electrons by the additional cobalt d electrons. For the $8f$ sites with less cobalt neighbors, the isomer shift remains quasiconstant which implies the location of cobalt in $8f$ sites. The hyperfine field at Fe site increases with cobalt content, whatever the site.

The increase in the isomer shifts of an individual iron site upon carbonation may be understood in terms of the increase in unit-cell volume and the presence of a carbon near neighbor for a specific site. Our assignment leads to a reasonable change in the isomer shifts of all sites upon carbonation. The carbides exhibit easy c-axis anisotropy throughout the temperature range due to the crystal field created at praseodymium produced by the pairs of carbon neighbors along the c axis. The average hyperfine fields of carbides are 12 to 5% for, respectively, $x=0$ and $x=3$ larger than those of the parent compounds at 77 K and at room temperature. The changes in hyperfine field upon carbonation of $PrTiFe_{11-x}Co_x$ are in agreement with the unit cell volume expansion.

[1] X.C. Kou, T.S. Zhao, R. Grössinger, H.R. Kirchmayr, X. Li, and F.R. de Boer, Phys. Rev. B **47**, 3231 (1993).
[2] K.H.J. Buschow, Rep. Prog. Phys. **54**, 1123 (1991).
[3] Z. Tang, E.W. Singleton, and G.H. Hadjipanayis, J. Appl. Phys. **73**, 6245 (1993).
[4] Y.C. Yang, Q. Pan, X.D. Zhang, M.H. Zhang, C.L. Yang, Y. Li, S. Ge, and B.F. Zhang, J. Appl. Phys. **74**, 4066 (1993).
[5] O. Kalogirou, V. Psycharis, L. Saettas, and D. Niarchos, J. Appl. Phys. **76**, 6722 (1994).
[6] Q. Qi, B.P. Hu, and J.M.D. Coey, J. Appl. Phys. **75**, 6235 (1994).
[7] K.H.J. Buschow, J. Magn. Magn. Mater. **100**, 79 (1991).
[8] Y.Z. Wang, L. Song, K.Y. Wang, B.P.H.G.C. Liu, and W.Y. Lai, J. Magn. Magn. Mater. **140**, 1019 (1995).
[9] R. Rani, H. Hegde, A. Navarathna, and F.J. Cadieu, J. Appl. Phys. **75**, 6006 (1994).
[10] Z.Q. Jin, W. Tang, J.R. Zhang, L.Y. Lu, S.L. Tang, and Y.W. Du, J. Magn. Magn. Mater. **187**, 231 (1998).
[11] Q. Zeng, Y.F. Xiao, S.Z. Dong, X.B. Liu, B.Q. Qiu, Z.Y. Zhang, and R. Wang, J. Magn. Magn. Mater. **192**, 321 (1999).
[12] M. Akayama, H. Fujii, K. Yamamoto, and K. Tatami, J. Magn. Magn. Mater. **130**, 99 (1994).
[13] S. Tang, J.H. Yin, Z.Q. Jin, J.R. Zhang, S.Y. Zhang, and Y.W. Du, J. Appl. Phys. **85**, 4687 (1999).
[14] D.P. Hurley and J.M.D. Coey, J. Phys.: Condens. Matter **4**, 5573 (1992).
[15] K.H.J. Buschow, D.B. de Mooij, M. Brouha, H.H.A. Smit, and R.C. Thiel, IEEE Trans. Magn. **24**, 1161 (1988).
[16] R. Vert, Ph.D. thesis, Université de Grenoble, 1999.
[17] H.M. Rietveld, Acta Crystallogr. **22**, 151 (1967).
[18] H.M. Rietveld, J. Appl. Crystallogr. **2**, 65 (1969).
[19] J. Rodríguez-Carvajal, Physica B **192**, 55 (1993).
[20] J. Rodríguez-Carvajal, M.T. Fernandez-Diaz, and J.L. Martinez, J. Phys.: Condens. Matter **3**, 3215 (1991).
[21] C. Djega-Mariadassou and L. Bessais, J. Magn. Magn. Mater. **210**, 81 (2000).
[22] L. Bessais and C. Djega-Mariadassou, Phys. Rev. B **63**, 054412 (2001).
[23] D.B. de Mooij and K. Buschow, J. Less-Common Met. **136**, 207 (1988).
[24] S.F. Cheng, V.K. Sinha, Y. Xu, J.M. Elbicki, E.B. Boltich, W.E. Wallace, S.G. Sankar, and D.E. Laughlin, J. Magn. Magn. Mater. **75**, 330 (1988).

[25] R. Skolozdra, E. Tomey, G. Gignoux, D. Fruchart, and J.L. Soubeyroux, J. Magn. Magn. Mater. **139**, 65 (1995).
[26] O. Moze, L. Pareti, M. Solzi, and W. Davis, Solid State Commun. **66**, 465 (1988).
[27] D.G. Pettifor, Physica B **149**, 3 (1988).
[28] Z.W. Li, X.Z. Zhou, and A.H. Morrish, J. Appl. Phys. **69**, 5602 (1991).
[29] S.M. Pan, H. Chen, Z.X. Xu, R.Z. Ma, J.L. Yang, B.S. Zhang, D.Y. Xue, and Q. Ni, J. Appl. Phys. **76**, 6720 (1994).
[30] Y. Yang, L. Kong, H. Sun, J. Yang, Y. Ding, B. Zhang, C. Ye, and L. Jin, J. Appl. Phys. **67**, 4632 (1990).
[31] J.J. Bara, B.F. Bogacz, A.T. Pedziwiatr, and R. Wielgosz, J. Alloys Compd. **307**, 45 (2000).
[32] D. Denissen, R. Coehoorn, and K. Buschow, J. Magn. Magn. Mater. **87**, 51 (1990).
[33] Z. Li, X. Zhou, and A. Morrish, J. Phys.: Condens. Matter **4**, 10409 (1992).
[34] J.M.D. Coey and Q. Qi, Hyperfine Interact. **90**, 265 (1994).
[35] Y. Yang, X. Zhang, L. Kong, S. Ge, J. Yang, Y. Ding, B. Zhang, C. Ye, and L. Jin, Solid State Commun. **78**, 313 (1991).
[36] D.P. Middleton, F.M. Mulder, R.C. Thiel, and K.H.J. Bushow, J. Magn. Magn. Mater. **146**, 123 (1995).
[37] B.P. Hu, H.S. Li, H. Song, and J.M.D. Coey, J. Phys.: Condens. Matter **3**, 3983 (1991).
[38] D.L. Williamson, S. Bukshpan, and R. Ingalls, Phys. Rev. B **6**, 4194 (1972).
[39] V. Heine, Phys. Rev. **153**, 673 (1967).
[40] S. Dong, J. Yang, and Y. Yang, Solid State Commun. **94**, 809 (1995).
[41] Q. Qi, D.Y. Li, and J.M.D. Coey, J. Phys.: Condens. Matter **4**, 8029 (1992).